Materials Chemistry and Physics 161 (2015) 194–200

Contents lists available at ScienceDirect

Materials Chemistry and Physics

journal homepage: www.elsevier.com/locate/matchemphys

First principle modeling of oxygen-doped monolayer graphitic carbon nitride

Jie Cui [a, b], Shuhua Liang [a, b, *], Xianhui Wang [a, b], Jianmin Zhang [c]

[a] School of Materials Science and Engineering, Xi'an University of Technology, Xi'an 710048, PR China
[b] Shaanxi Province Key Laboratory for Electrical Materials and Infiltration Technology, Xi'an University of Technology, Xi'an 710048, PR China
[c] College of Physics and Information Technology, Shaanxi Normal University, Xi'an 710062, PR China

HIGHLIGHTS

- We reveal the favorable O doping configurations over all the Fermi levels.
- O doping facilitates the visible-light absorption of monolayer g-C_3N_4.
- O doping causes slightly stronger delocalization of the HOMO and LUMO.

ARTICLE INFO

Article history:
Received 19 December 2014
Received in revised form
2 April 2015
Accepted 13 May 2015
Available online 18 May 2015

Keywords:
Monolayers
Ab initio calculations
Band-structure
Electronic structure

ABSTRACT

The effect of oxygen doping on the electronic and geometric structures of monolayer graphitic carbon nitride was calculated by first principle. It reveals the favorable O doping configurations over all the Fermi levels utilizing the *Ab initio* thermodynamics approach. The valence charge density difference contour map presents a weaker covalent nature on O–C bonds for O_{N2}-doped structure and a complex ionic-covalent character associated with O–N2 bonds for O_i-doped structure. Based on the analysis of the electronic structures of the doped and un-doped systems, it is found that O doping facilitates the visible-light absorption of monolayer g-C_3N_4. Especially, O_i doping shows an intrinsic semiconductor behavior and the occupied doping band can be avoided to be the recombination center. In addition, O doping causes slightly stronger delocalization of the HOMO and LUMO which facilitates the enhancement of the carrier mobility. Moreover, O_i doping can induce more activity sites, and, thus, is beneficial for the separation of photogenerated e^-/h^+ pairs to some extent.

1. Introduction

With crisis of energy resources and increased environmental pollution, more attentions have been paid on the development of semiconductor photocatalysts. Titanium dioxide is one of the widest used photocatalysts due to its abundance, low-cost, low-toxicity and superior photo-stability [1,2]. However, it can only be activated by UV light irradiation, which greatly limits its wide applications. To utilize solar energy in a more efficient way, the design and preparation of visible light active photocatalysts is highly expected and has been one of the most important issues in catalyst research.

As a stable metal-free photocatalyst, the heptazine-based graphitic carbon nitride (g-C_3N_4) has been recently considered as a promising photocatalyst for hydrogen production through photoelectrochemical (PEC) water splitting. Wang et al. [3] reported on a cross-linked g-C_3N_4 polymeric semiconductor, which can produce hydrogen from water under visible-light irradiation in the presence of a sacrificial donor. Nevertheless, low carrier mobility and insufficient sunlight absorption limit the energy conversion efficiency. In recent years, considerable efforts have been devoted to improve the photocatalytic performance of g-C_3N_4 and various strategies have been developed to address this issue, including nanostructure engineering, mesostructure introduction, metal/non-metal doping, semiconductor compositing and noble metal deposition [4–8,16].

Surface area plays an important role in enhancing mass transfer and offering more active sites. Moreover, the shorter diffusion path for higher surface area materials is advantageous to suppress the recombination of photo-generated charges. Thus, more attentions

* Corresponding author. Shaanxi Province Key Laboratory for Electrical Materials and Infiltration Technology, Xi'an University of Technology, Xi'an 710048, PR China.
E-mail address: liangsh@xaut.edu.cn (S. Liang).

http://dx.doi.org/10.1016/j.matchemphys.2015.05.036
0254-0584/

are paid on the nano-/hollow-structured materials with high surface area [6–11]. Among them, the processing, properties, and applications of g-C_3N_4 nanosheet have been widely studied. For example, g-C_3N_4 nanosheets with a thickness of about 2 nm were prepared successfully by thermal oxidation etching of bulk g-C_3N_4 in air. Compared with the bulk g-C_3N_4, the photoreactivity of g-C_3N_4 nanosheets is remarkably improved in terms of OH radical generation and photocatalytic hydrogen evolution [6]. Lin et al. [7] developed a versatile and scalable mixed solvent strategy for liquid exfoliation of bulk g-C_3N_4 to produce monolayer g-C_3N_4 nanosheet, and the as-prepared monolayer g-C_3N_4 shows distinctive physicochemical properties and unique electronic structures. Besides this method, doping is also regarded as an effective strategy to improve the photocatalytic performance of g-C_3N_4 [12–16]. Li et al. [16] reported that O-doped g-C_3N_4 exhibits superior photoreactivity towards methyl blue degradation and H_2 evolution under visible light irradiation.

The calculation based on the density functional theory (DFT) is favorable to recognize the microscopic mechanism underlying the doping effects on the properties of interest of g-C_3N_4 [17–19]. The substitution of the nitrogen atom at the edge of the tri-*s*-triazine units with sulfur is an energetically favorable scenario. Meanwhile, a P atom preferentially situates the interstitial sites of g-C_3N_4 [17]. However, the oxygen atom has a smaller radius and higher electronegativity, and thus the doping effect and designing way are different from the existing nonmetal elements doping. Subsequently, it is of significance to understand the oxygen doping effect for the rational modification of the properties of g-C_3N_4 by doping and is helpful for the design and preparation of highly efficient visible-light photocatalysts.

In the present work, the effect of oxygen doping on the electronic and geometric structures of monolayer g-C_3N_4 was simulated by first principle method, starting with a brief overview on the monolayer g-C_3N_4 and then O doped as follows. The purpose of the investigation is to get more insights into the mechanism underlying the doping effects by a systematic survey of the geometric and electronic structures of O-doped monolayer g-C_3N_4. This paper is organized as follows. The details of the calculation method are given in Sec. 2. Electronic structures of monolayer g-C_3N_4; formation energies, geometric and electronic structures of oxygen-doped monolayer g-C_3N_4 are given in Sec. 3. The conclusions of this work are summarized in Sec. 4.

2. Calculations method

To understand the effects produced by O-doping in monolayer g-C_3N_4, the geometric and electronic structure was calculated based on the density functional theory (DFT) for pure monolayer g-C_3N_4 and monolayer with various doping configurations, using the VASP package [20]. The calculations used frozen-core projector-augmented wave (PAW) method [21] within the generalized gradient approximation (GGA) of Perdew et al. [22]. A kinetic energy cutoff of 450eV was used, a supercell geometry with 56 atoms in the cell was employed, a $3 \times 3 \times 1$ grid of special *k*-points for integrations over the Brillouin zone was proposed, and a more refined $7 \times 7 \times 1$ k-points mesh was used for the density of states (DOS). The results of the calculations were checked for convergence with respect to the cutoff energy and the k-points mesh.

The most stable pure g-C_3N_4, composed of nitrogen-linked heptazine units, is hexagonal with space group Cmcm [23]. As shown in Fig. 1, the basic in-plane building block consists of 3-fold coordinated C atoms, 3-fold coordinated bridge and inner and N atoms, 2-fold coordinated edge N atoms. Before the doping calculations, the crystal parameters of pure g-C_3N_4 were calculated firstly and the results of in-plane lattice constant $a = 7.14$ Å is in agreement with the experimental value $a = 7.13$ Å [6]. The interlayer distance

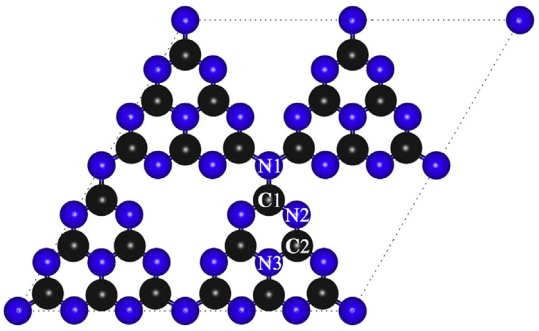

Fig. 1. Initial atomic structure of hexagonal heptazine-based g-C_3N_4 sheet. Black and blue spheres represent the C and N atoms, respectively. Roman numbers labeled on the C and N atoms are used to identify the special sites. (For interpretation of the references to color in this figure legend, the reader is referred to the web version of this article.)

$c = 6.94$ Å is almost equal to the theoretical results reported by Ma [17] and Gracia [24], but the value is larger than the experimental value [3,25]. The difference may be derived from the GGA and the semi-empirical approximation for the van der Waals forces between layers, which does not cause any remarkable effect on the electronic structure of the system. The calculated band gap (1.18 eV) is much smaller than the experimental result (2.7 eV), due to the failure of GGA to describe the relative energies of occupied and unoccupied electron levels. Being a covalent compound, the GGA + U approach failed to correct the band gap of g-C_3N_4 system. Though the hybrid approach can give the right band gap of g-C_3N_4 system, it takes a much longer time to achieve the goal, which limits its widespread adoption on the electronic structure calculation of g-C_3N_4 [17,19]. The magnitude of the band gap is underestimated in the present work, but the calculations can still support the interpretation of the photocatalytic activity.

3. Results and discussions

3.1. Electronic structures of monolayer g-C_3N_4

In order to study the effect of the quantum confinement effect, the electronic structures of monolayer g-C_3N_4 were calculated. A relatively large vacuum distance of about 15 Å between layers was

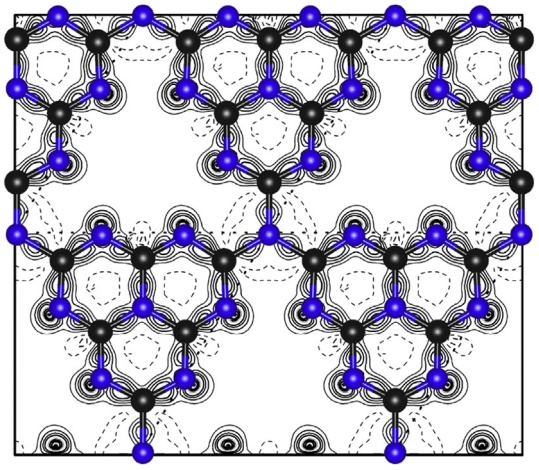

Fig. 2. The calculated charge density difference contour map for (001) lattice plane of monolayer g-C_3N_4. Black and blue spheres represent the C and N atoms, respectively. The solid line represents the positive charge density and the dashed line negative charge density. (For interpretation of the references to color in this figure legend, the reader is referred to the web version of this article.)